

High cadence observations of a global coronal wave by EUVI/STEREO

Astrid M. Veronig

*Institute of Physics/IGAM, University of Graz, Universitätsplatz 5, A-8010 Graz, Austria;
asv@igam.uni-graz.at*

Manuela Temmer

*Space Research Institute, Austrian Academy of Sciences, Schmiedlstraße 6, A-8042 Graz,
Austria; manuela.temmer@uni-graz.at*

Bojan Vršnak

*Hvar Observatory, Faculty of Geodesy, Kačićeva 26, HR-10000 Zagreb, Croatia;
bvrsnak@geodet.geof.hr*

ABSTRACT

We report a large-scale coronal wave (so-called “EIT wave”) observed with high cadence by EUVI onboard STEREO in association with the GOES B9.5 flare and double CME event on 19 May 2007. The EUVI instruments provide us with the unprecedented opportunity to study the *dynamics* of flare/CME associated coronal waves. The coronal wave under study reveals deceleration, indicative of a freely propagating MHD wave. Complementary analysis of the associated flare and erupting filament/CME hint at wave initiation by the CME expanding flanks, which drive the wave only over a limited distance. The associated flare is very weak and occurs too late to account for the wave initiation.

Subject headings: shock waves — Sun: corona — Sun: flares

1. Introduction

Large-scale large-amplitude waves and shocks in the solar corona occur in association with flares and coronal mass ejections (CMEs). The existence of flare-related global disturbances has been first inferred from Moreton waves (Moreton & Ramsey 1960), which appear as arc-like fronts in chromospheric H α filtergrams, moving away from the ignition site with typical velocities of 500–1000 km/s. It was soon recognized that Moreton waves could not

be propagating in the chromosphere, where no wave mode has such high velocity (e.g. sound speed and Alfvén speed are only of the order of tens of km/s). The first interpretation was by Uchida (1968) that Moreton waves are the surface-track of a coronal fast-mode magnetohydrodynamic (MHD) wave front.

The Extreme-ultraviolet (EUV) Imaging Telescope (EIT; Delaboudinière et al. 1995) onboard Solar and Heliospheric Observatory (SOHO) for the first time directly imaged propagating global disturbances in the corona, and these so-called “EIT waves” were assumed to be the coronal counterparts of the Moreton waves (Thompson et al. 1998, 1999). Thereafter, coronal waves were found to be a quite frequent phenomenon, and it became an intense matter of debate whether EIT waves:

- a) are really the coronal counterparts of Moreton waves (e.g. Thompson et al. 2000; Klassen et al. 2000; Warmuth et al. 2001, 2004a; Eto et al. 2002; Khan & Aurass 2002; Narukage et al. 2002; Vršnak et al. 2002; Gilbert et al. 2004; Veronig et al. 2006);
- b) are caused by the flare explosive energy release or by the erupting CME (e.g. Warmuth et al. 2001, 2004b; Biasecker et al. 2002; Hudson et al. 2003; Zhukov & Auchère 2004; Cliver et al. 2005; Vršnak et al. 2006);
- b) are waves at all (and, if yes, which type of waves; cf. Wills-Davey et al. 2007) or rather propagating disturbances related to magnetic field line opening and restructuring associated with the CME lift-off (e.g. Delannée & Aulanier 1999; Wills-Davey & Thompson 1999; Delannée 2000; Wang 2000; Wu et al. 2001; Warmuth et al. 2001; Chen et al. 2002; Vršnak et al. 2002; Ballai et al. 2005; Attrill et al. 2007).

In addition, there might be different types of EIT waves, further complicating this debate. For detailed discussions we refer to the recent reviews by Chen and Fang (2005); Vršnak (2005); Mann (2007); Warmuth (2007).

One important limitation of coronal wave studies so far is the low cadence of the EIT instrument (12–15 min), which makes it impossible to study wave kinematics beyond a rough velocity estimate. Observations of large-scale waves in TRACE EUV images are rare due to its limited field of view, but we note that one such event was observed with high cadence and studied in detail in Wills-Davey & Thompson (1999). The Extreme Ultraviolet Imagers (EUVI) on the recent Solar Terrestrial Relations Observatory (STEREO) spacecraft regularly perform EUV full-disk imaging with a cadence as good as 2.5 min. In this letter, we study for the first time the dynamical evolution of a globally propagating “EIT” wave in high-cadence EUVI images.

2. Data

EUVI is part of the Sun Earth Connection Coronal and Heliospheric Investigation (SECCHI; Howard et al. 2008) instrument suite onboard STEREO (Kaiser et al. 2008). STEREO consists of two identical spacecraft, which orbit the Sun ahead (STEREO-A) and behind (STEREO-B) the Earth near the ecliptic plane. EUVI is observing the chromosphere and low corona in four EUV bandpasses (He II 304 Å, Fe IX 171 Å, Fe XII 195 Å, Fe XV 284 Å) out to $1.7 R_s$ (with R_s the solar radius) with a pixel limited spatial resolution of $1.6''/\text{pixel}$. During the event under study, the EUVI imaging cadence was 2.5 min in the 171 Å and 10 min in the 195 Å filter.

The impulsive phase of the associated B9.5/SF flare was fully captured in hard X-rays by the Ramaty High Energy Spectroscopic Imager (RHESSI; Lin et al. 2002). For the study of associated CMEs, we use data from the STEREO/SECCHI inner coronagraph COR1, which has a field-of-view (FOV) from 1.4 to $4 R_s$ (Howard et al. 2008), and from the Large Angle Spectroscopic Coronagraph (LASCO; Brueckner et al. 1995) onboard SOHO.

3. Results

3.1. Kinematics and dynamics of the coronal wave

The coronal wave under study occurred on 19 May 2007 during $\approx 12:50\text{--}13:20$ UT, in association with the weak B9.5 flare/CME event in AR 10956 close to Sun center ($N01^\circ, W05^\circ$). The two STEREO spacecraft were 8.6° apart and both observed the wave. We concentrate on STEREO-A observations, since it observed a larger portion of the Western solar hemisphere, into which the wave propagated. For comparison of STEREO-A images with other space-borne and ground-based data, we rescaled the image sizes to Earth distance. On 19 May 2007, STEREO-A was at a distance of 0.96 AU from Sun, and Earth was at 1.01 AU. Thus, we decreased the angular diameter of the STEREO-A images by 5.4%.

Figures 1 and 2 show running ratio images (i.e. each image is divided by the previous one) of the coronal wave observed in the EUVI 195 Å and 171 Å passband, respectively. The coronal wave fronts could be identified and measured in 7 images taken in the 171 Å and 4 images in the 195 Å filter during a period of ≈ 30 min. The wave shows global propagation (see 195 Å image at 13:02 UT) but is most pronounced towards W and NW. The wave “radiant point” was estimated by applying circular fits to the two earliest wave fronts observed in 171 and 195 Å after transforming the data from the 2D cartesian xy -plane to the 3D spherical $r\theta\phi$ -plane (solar radius, heliographic latitude and longitude). The center of

curvature of the wave was found on the NW border of AR 10956. In Fig. 3, the determined wave centers together with the strongest wavefront segments are plotted. In contrast to Moreton waves, 360° propagation is not uncommon for coronal waves (e.g., discovery event of Thompson et al. 1998). Simulations by Ofman & Thompson (2002) revealed that the wave is strongly refracted/reflected by ARs, but part of it can pass through. If the AR is small, the wave can be diffracted into the region behind the AR (passing above and aside), which may be the case in the event under study. We also note that the wave was refracted and reflected at the coronal hole in the SW solar quadrant (cf. Fig. 3).

Figure 4 shows the distance-time diagram of the wave derived by calculating the mean distance of the wave fronts from the wave center along great circles on the lower corona, where the EUVI wave is observed (estimated to be 10 Mm above the photosphere). For the kinematics, we used only the strongest wavefront segments (at 13:02 UT the global wave front) shown in Fig. 3. The linear fit to the distance-time diagram gives a mean wave velocity of 260 km s^{-1} . The quadratic fit yields a start velocity of 460 km s^{-1} , a (constant) deceleration of -160 m s^2 and an extrapolated wave launch time (intersect with x -axis) of 12:45 UT. The inset in Fig. 4 shows the wavefront velocity derived by numerical derivative of the measured time-distance data using 3-point linear interpolation, together with the applied fits. The velocity evolution demonstrates that the wave decelerates, with the earliest velocities as high as $400\text{--}500 \text{ km s}^{-1}$. This is considerably faster than the velocities reported for EIT waves ($170\text{--}350 \text{ km s}^{-1}$; Klassen et al. 2000), which we attribute to the much better cadence of EUVI, allowing us to study the wave’s evolution.

Up to now, deceleration of coronal waves was mainly hypothesized from the deceleration observed in chromospheric Moreton waves recorded with high cadence, and from their combination with (mostly single) EIT wave fronts lying on the extrapolated kinematical curve of the decelerating Moreton wave (Warmuth et al. 2001, 2004a; Vršnak et al. 2002). Evidence for deceleration of coronal waves was provided also from soft X-ray imaging in Warmuth et al. (2005). However, in the coronal wave studied in Wills-Davey & Thompson (1999) the general picture was quite different in that some parts of the wave fronts showed acceleration. Initial acceleration of the wave is actually expected from the theoretical point of view (see Fig. 4 in Vršnak & Lulić 2000).

3.2. Dynamics of the associated eruptions

The LASCO/SOHO catalog (Yashiro et al. 2004) reports two CMEs in association with the coronal wave under study: CME1 was observed at a position angle PA of 260° in the FOV $3\text{--}20 R_s$ with a mean velocity of 960 km s^{-1} , CME2 at PA 310° in the FOV $3\text{--}10 R_s$ with

290 km s⁻¹. Both CMEs were rather poor events, but associated with an interplanetary magnetic cloud observed in situ at ≈ 1 AU on 21/22 May 2007 by STEREO and Wind (Liu et al. 2008). COR1 on STEREO-A did not observe the fast CME1 (which was very faint) but it observed the evolution of CME2 in the low corona. The linear fit gives a mean CME2 velocity of 430 km s⁻¹ in the FOV 1.5–2.5 R_s ; the quadratic fit gives a start velocity of 650 km s⁻¹ at 12:48 UT, and a deceleration of -90 m s².

In Fig. 5 we plot a sequence of H α filtergrams which show the earliest sign of the eruption, two erupting filaments. Their orientation and direction is consistent with the position angles of the two CMEs. Filament1 (towards W) has disappeared from the H α filter at 12:46 UT, filament2 (towards NW) at 12:55 UT (see Fig. 5). The filament evolution appears more complex in EUVI 171 Å images, with fast changes/eruption of the filament system starting between 12:49:00 and 12:51:30 UT.

4. Discussion and Conclusions

In Figure 6, we show a summary plot comprising: a) the distance-time diagram of the coronal wave observed by EUVI/STEREO-A, b) the back-extrapolated (quadratic fit) distance-time diagram of CME1 observed with LASCO/SOHO, c) the distance-time diagram of CME2 observed with COR1/STEREO-A, d) the flare hard X-ray flux recorded by RHESSI, and e) the flare soft X-ray flux recorded by GOES. From the quadratic fit to the EUVI wave kinematics, we estimate the wave’s launch time to $\approx 12:45$ UT. The real launch may happen somewhat later, since this method assumes a point-like origin of the wave. The flare 12–25 keV hard X-ray flux starts rising at 12:50 UT with the first and highest peak at 12:51:30 UT. At this time, we already observe the first EUVI wave front. Such timing argues against a flare-origin of the wave, since the wave needs time to build up a large amplitude or shock to be observable. On the other hand, timing and direction of the erupting filaments indicate that the wave was closely associated with the fast CME1, since filament1 disappeared from the H α filter at 12:46 UT, whereas filament2 remained visible until 12:55 UT.

However, the kinematics of the coronal wave is quite different from the kinematics of the CME’s leading edge (see Fig. 6): the wave is slower than both CMEs and significantly decelerates, which is a typical characteristics of a large-amplitude MHD simple wave (Mann 1995; Vršnak & Lulić 2000): such a freely propagating perturbation is powered only temporarily by a source region expansion, which could be due to the flare-related pressure pulse, due to small scale flare ejecta or due to the CME expanding flanks (which propagate laterally only over a limited distance). Since perturbation elements with larger amplitude travel faster than those with smaller amplitude (nonlinearity), the perturbation profile steepens

until finally a discontinuity is formed. As a consequence of energy conservation, the amplitude of the perturbation decreases with distance, first due to spherical expansion ($\sim R^{-2}$), and second, because the crest of the shock travels faster than its trail, causing broadening of the perturbation profile (Landau & Lifshitz 1987). Consequently, the wave decays into an ordinary, i.e. small amplitude wave propagating with the characteristic speed of the medium. For waves propagating perpendicular to the magnetic field, this is the magnetosonic speed $v_{\text{ms}} = (v_A^2 + c_s^2)^{1/2}$ with v_A the Alfvén velocity and c_s the sound speed. The “final” velocity reached by the EUVI wave under study lies in the range $200 \pm 50 \text{ km s}^{-1}$ (see Fig. 4), which is a reasonable value of v_{ms} in the quiet solar corona (e.g., Mann et al. 1999), though we note that there is an ongoing discussion on this subject (e.g. Wang 2000; Wu et al. 2001; Chen et al. 2002; Wills-Davey et al. 2007).

The observed EUVI wave deceleration together with the closely related timing of the wave and the erupting filament1/CME1 (in contrast to the flare peak which occurs too late) as well as the wave front shape which is roughly concentric with filament1, hint at an initiation of the wave by the CME expanding flanks. In such a scenario, the wave is only driven over a limited distance and then decays into an ordinary MHD wave.

We thank the SOHO, LASCO, STEREO, EUVI, and RHESSI teams for their open data policy, and the referee for his/her constructive comments. This work was supported by the Austrian Science Fund (FWF grants P20145-N16 and P20867-N16).

REFERENCES

- Attrill, G. D. A., et al. 2007, *ApJ*, 656, L101
- Ballai, I, Erdélyi, R., & Pintér, B. 2005, *ApJ*, 633, 145
- Biesecker, D. A., et al. 2002, *ApJ*, 569, 1009
- Brueckner, G. E., et al. 1995, *Sol. Phys.*, 162, 357
- Chen, P. F., et al. 2002, *ApJ*, 572, L99
- Chen, P. F., & Fang, C. 2005, *Proc. IAU Symp.*, 226, 55
- Cliiver, E. W., et al. 2005, *ApJ*, 631, 604
- Delaboudinière, J. P., et al. 1995, *Sol. Phys.*, 162, 291
- Delannée, C., & Aulanier, G. 1999, *Sol. Phys.*, 190, 107

- Delannée, C. 2000, *ApJ*, 545, 512
- Eto, S. et al. 2002, *PASJ*, 54, 481
- Gilbert, H. R., et al. 2004, *ApJ*, 607, 540
- Howard, R. A., et al. 2008, *Space Sci. Rev.*, in press
- Hudson, H. S., et al. 2003, *Sol. Phys.*, 212, 121
- Liu, Y., et al. 2008, *ApJ*, 667, L133
- Kaiser, M. L., et al. 2008, *Space Sci. Rev.*, in press
- Khan, J. I. & Aurass, H. 2002, *A&A*, 383, 1018
- Klassen, A., et al. 2000, *A&AS*, 141, 357
- Landau, L. D., & Lifshitz, E. M. 1987, *Fluid mechanics*, 2nd ed., Oxford: Pergamon Press
- Lin, R. P., et al. 2002, *Sol. Phys.*, 210, 3
- Mann, G. 1995, *J. Plasma Phys.*, 53, 109
- Mann, G. 2007, *Geophys. Monograph Ser.* 165, 221
- Mann, G., et al. 1999, *ESA-SP*, 446, 477
- Moreton, G. E. & Ramsey, H. E. 1960, *PASP*, 72, 357
- Narukage, N., et al. 2002, *ApJ*, 572, L109
- Ofman, L., & Thompson, B. J. 2002, *ApJ*, 574, 440
- Otruba, W., & Pötzi, W. 2005, *Hvar Obs. Bull.*, 27, 198
- Thompson, B. J., et al. 1998, *Geophys. Res. Lett.*, 25, 2465
- Thompson, B. J., et al. 1999, *ApJ*, 517, L161
- Thompson, B. J., et al. 2000, *Sol. Phys.*, 193, 161
- Uchida, Y. 1968, *Sol. Phys.*, 4, 30
- Veronig, A.M., et al. 2006, *A&A*, 446, 675
- Vršnak, B. 2005, *EOS Transactions*, 86, 112

- Vršnak, B., & Lulić, S. 2000, *Sol. Phys.*, 196, 157
- Vršnak, B., et al. 2002, *A&A*, 394, 299
- Vršnak, B., et al. 2006, *A&A*, 448, 739
- Wang, Y.-M. 2000, *ApJ*, 543, L89
- Warmuth, A. 2007, *Lecture Notes in Physics*, 725, 107
- Warmuth, A., et al. 2001, *ApJ*, 560, L105
- Warmuth, A., et al. 2004a, *A&A*, 418, 1101
- Warmuth, A., et al. 2004b, *A&A*, 418, 1117
- Warmuth, A., Mann, G., & Aurass, H. 2005, *A&A*, 626, L121
- Wills-Davey, M. J., DeForest, C. E., & Stenflo, J. O. 2007, *ApJ*, 664, 556
- Wills-Davey, M. J., & Thompson, B. J. 1999, *Sol. Phys.*, 190, 467
- Wu, S. T., et al. 2001, *J. Geophys. Res.*, 106, 25089
- Yashiro, S., et al. 2004, *J. Geophys. Res.*, 109, 705, Issue A7, CiteID A07105
- Zhukov, A. N., & Auchère, F. 2004, *A&A*, 427, 705

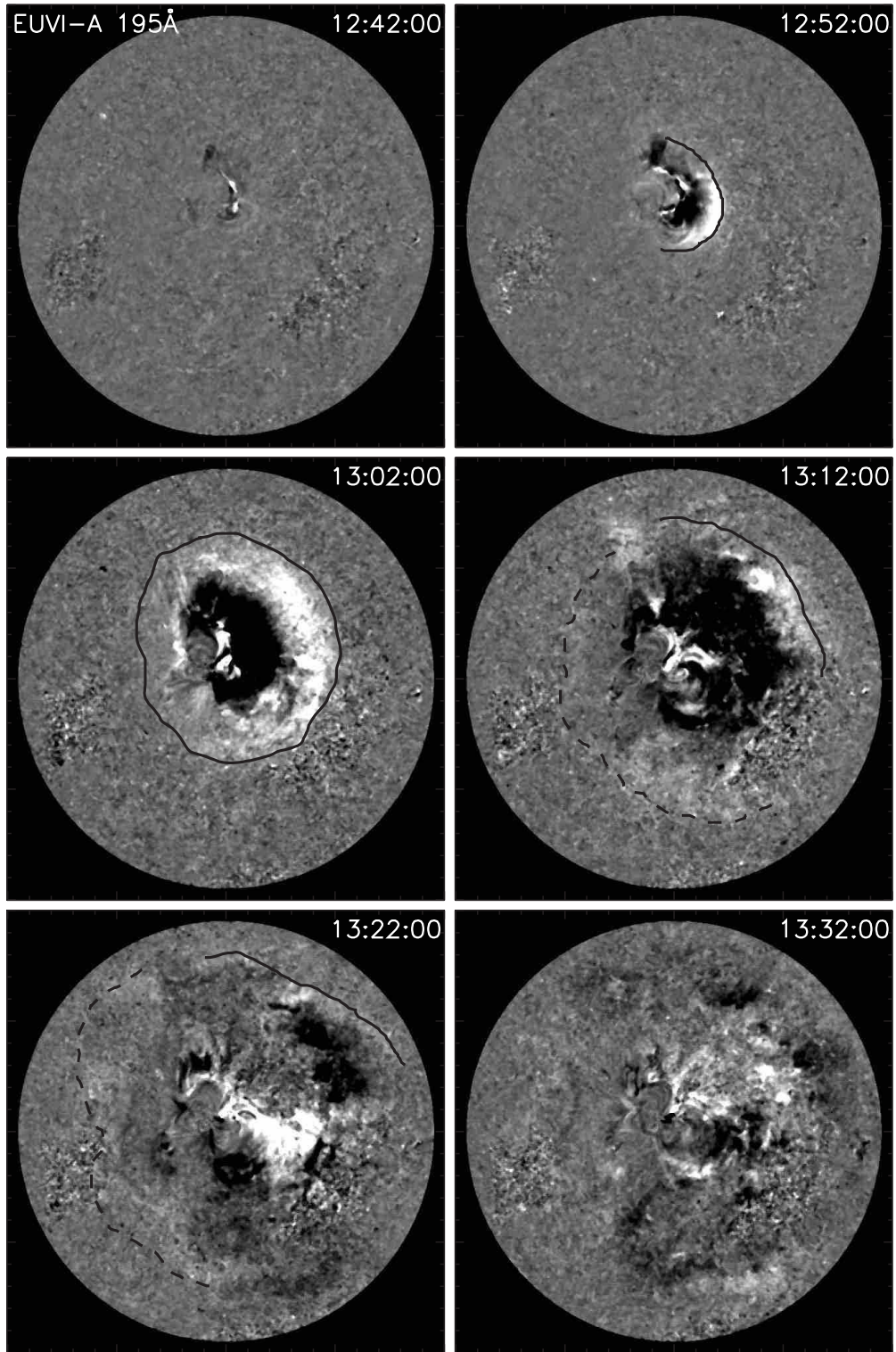


Fig. 1.— Sequence of median-filtered running ratio images recorded in the EUVI/STEREO-A 195 Å channel with a cadence of 10 min. The identified front edges of the wave are indicated with black lines. Only the strongest wave front segments (full lines) are considered in the kinematical plot in Fig 4. The plotted FOV is $2000'' \times 2000''$ around Sun center.

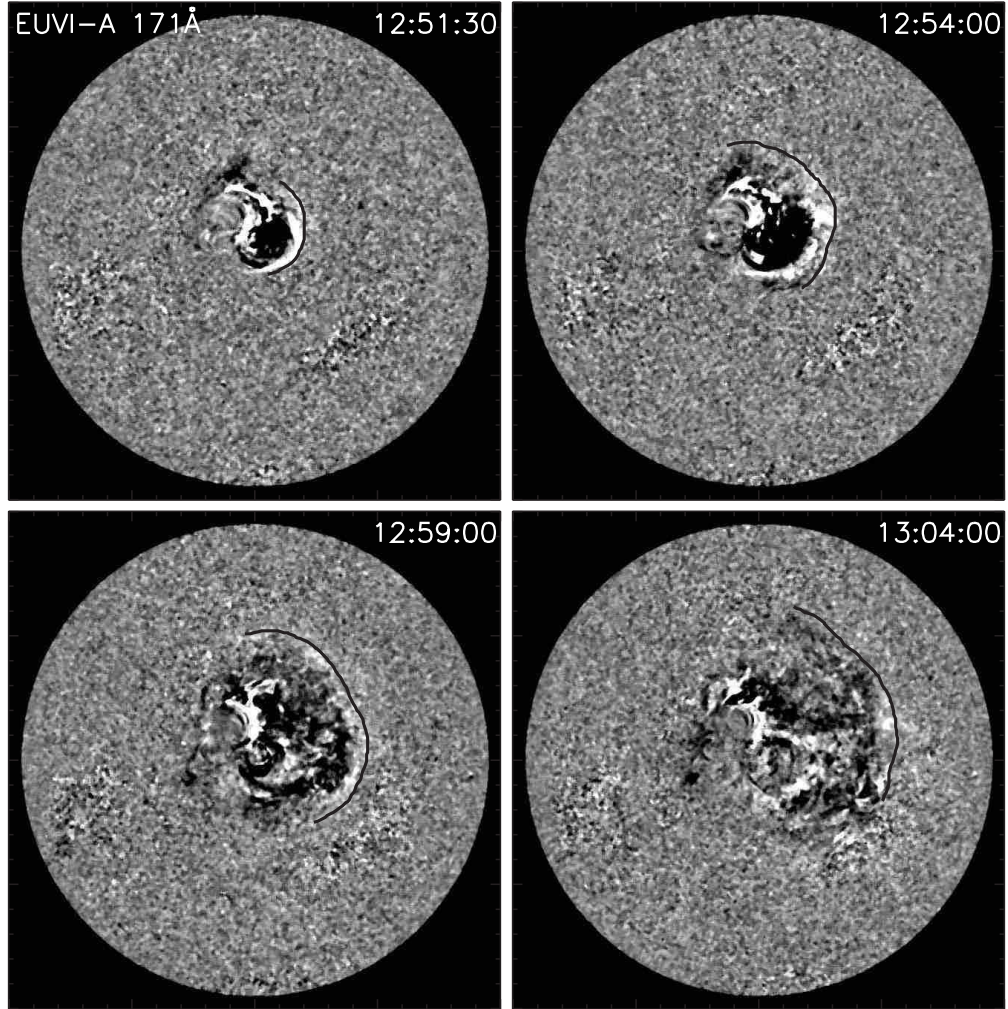


Fig. 2.— Same as Fig. 1 but for the EUVI 171 Å channel. Not all images in which the wave can be identified (2.5 min cadence) are shown.

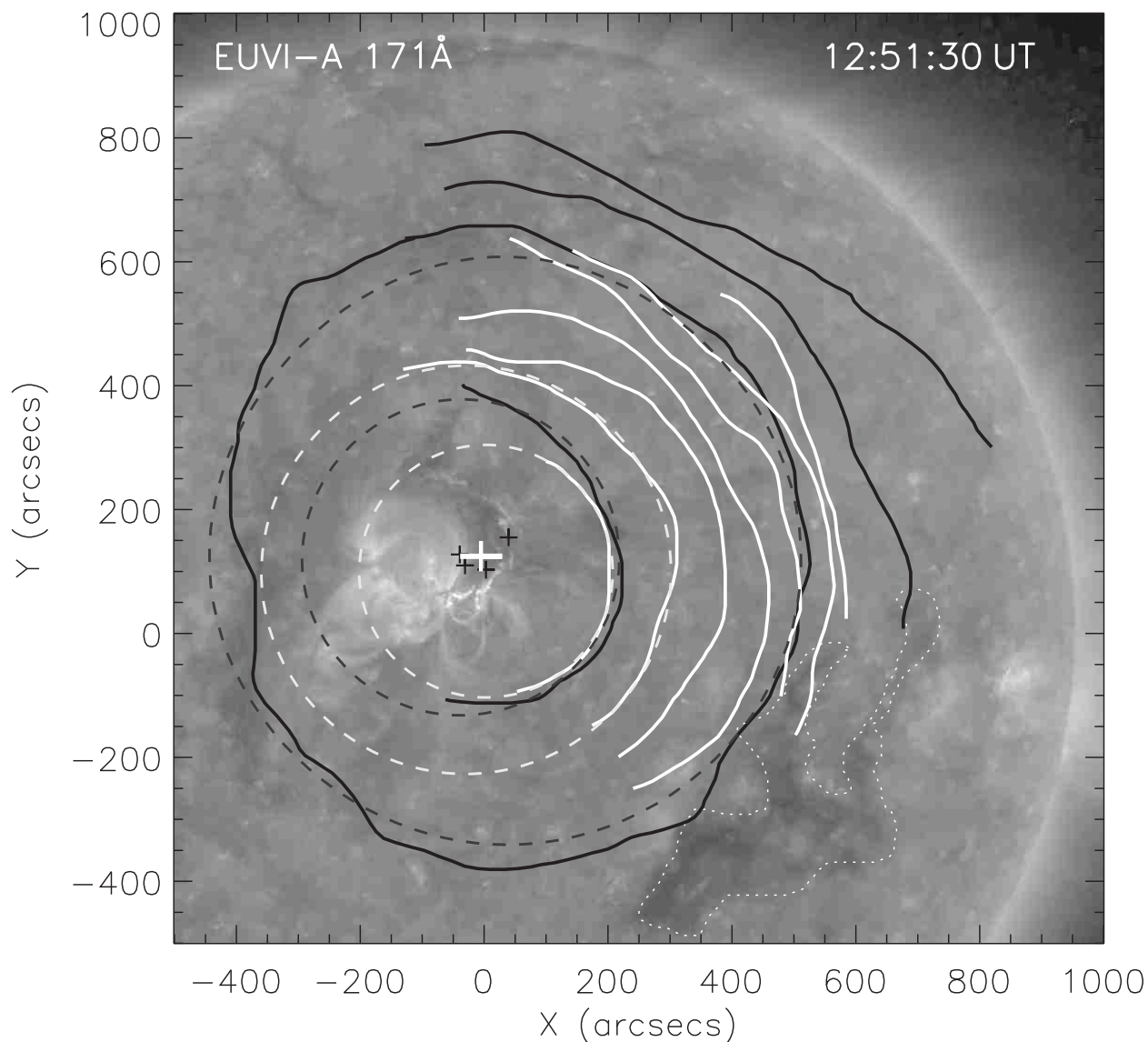


Fig. 3.— Section of an EUVI 171 Å image. The full lines mark the wave fronts identified in 171 Å (white) and 195 Å (black) images (cf. Figs. 1 and 2). The dashed lines indicate the circular fits to the two earliest wave fronts observed in 171 and 195 Å, respectively, which appear as ellipses in the 2D projected solar image. The wave centers derived by this method (black crosses) lie at the NW edge of AR 10956. The white cross marks the mean of the individual wave centers derived: $[x_c, y_c] = [-7'', 123''] \pm [40'', 20'']$. The dotted curve outlines the border of a nearby coronal hole, where the wave is refracted and reflected.

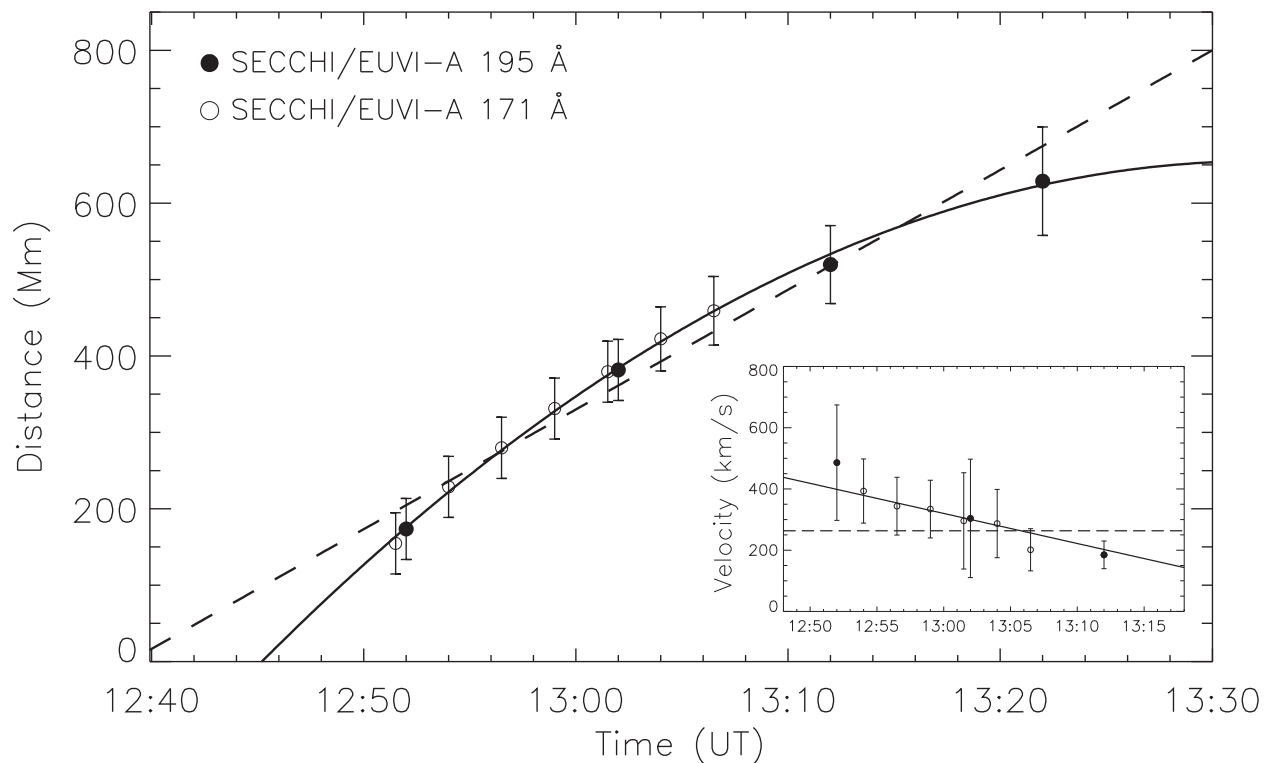


Fig. 4.— Kinematics of the coronal wave observed by EUVI/STEREO-A: Combined distance vs. time diagram derived from the wave fronts observed in 195 Å and 171 Å. The error bars reflect uncertainties on the calculated wave center as well as on the identification of the wave fronts. The dashed, gray and black lines indicate the linear and quadratic least-squares fits to the time-distance data, respectively. The inset shows the velocity evolution derived by numerical derivative using 3-point linear interpolation (error bars are due to uncertainties in the wave front determination).

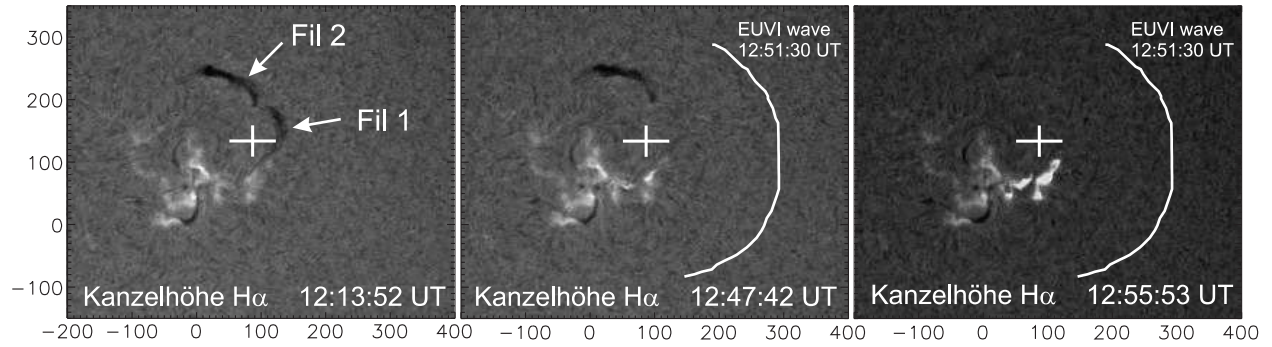


Fig. 5.— Sequence of H α filtergrams recorded at Kanzelhöhe Observatory showing the two erupting filaments. For comparison, we also plot the first EUVI wavefront (12:51:30 UT) and the derived wave ignition center, which have been transformed by $+5.7^\circ$ in longitude and $+0.7^\circ$ in latitude in order to account for the different view from STEREO-A with respect to Earth. Coordinates are in arcsec.

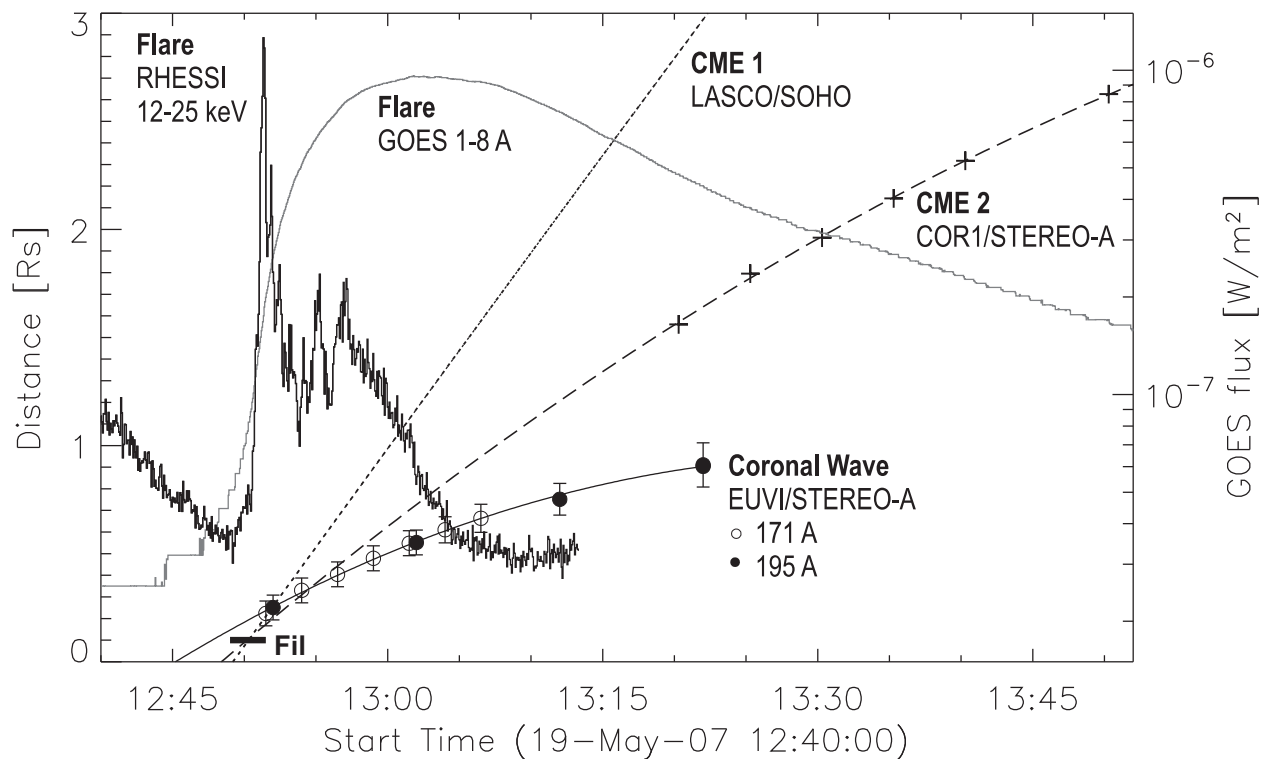


Fig. 6.— Summary plot of the coronal wave kinematics (measured distances: circles; quadratic fit: full lines) together with the flare evolution (GOES 1–8 Å soft X-ray flux: gray curve; RHESSI 12–25 keV hard X-rays: black spiky curve) and kinematics of CME2 observed in COR1/STEREO (pluses; together with quadratic fit) and the back-extrapolated quadratic fit of CME1 observed by LASCO/SOHO (dotted curve). The horizontal bar indicates the start of the fast filament eruption observed by EUVI.